Direct Exchange Mechanism for Interlayer Ions in Non-Swelling Clays

Luis Ruiz Pestana,[†] Kedarnath Kolluri,[‡] Teresa Head-Gordon,[†,§] and Laura Nielsen Lammers[*,‡,∥]

[†] Chemical Sciences Division and [‡] Earth and Environmental Science Area, Lawrence Berkeley National Laboratory, Berkeley, California 94720, United States [§] Departments of Chemistry, Bioengineering, Chemical and Biomolecular Engineering, and [∥] Department of Environmental Science, Policy, and Management, University of California, Berkeley, California 94720, United States

Corresponding Author *e-mail: lnlammers@berkeley.edu

Abstract

The mobility of radiocesium in the environment is largely mediated by cation exchange in micaceous clays, in particular Illite—a non-swelling clay mineral that naturally contains interlayer K^+ and has high affinity for Cs^+. Although exchange of interlayer K^+ for Cs^+ is nearly thermodynamically nonselective, recent experiments show that direct, anhydrous Cs^+-K^+ exchange is kinetically viable and leads to the formation of phase-separated interlayers through a mechanism that remains unclear. Here, using classical atomistic simulations and density functional theory calculations, we identify a molecular-scale positive feedback mechanism in which exchange of the larger Cs^+ for the smaller K^+ significantly lowers the migration barrier of neighboring K^+, allowing exchange to propagate rapidly once initiated at the clay edge. Barrier lowering upon slight increase in layer spacing (~0.7 Å) during Cs^+ exchange is an example of “chemical-mechanical coupling” that likely explains the observed sharp exchange fronts leading to interstratification. Interestingly, we find that these features are thermodynamically favored even in the absence of a heterogeneous layer charge distribution.

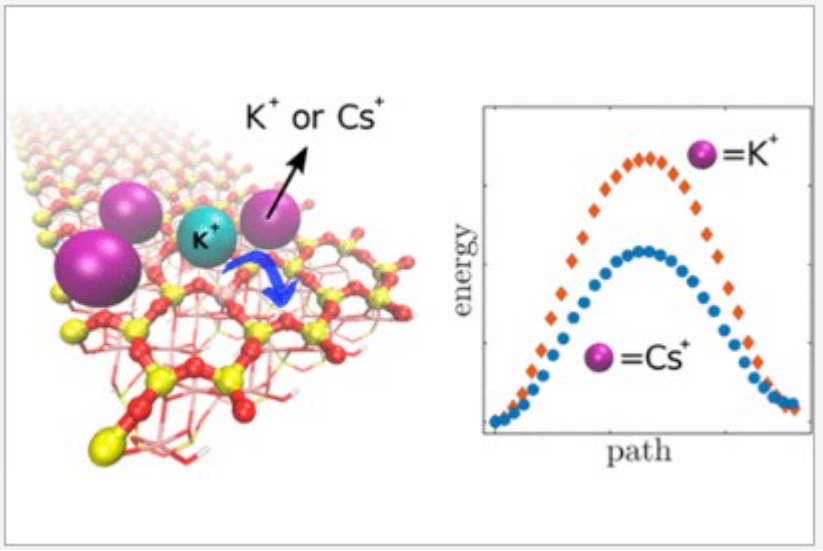

Introduction

Ion exchange in layered silicate minerals mediates contaminant immobilization,(1-11) weathering of micaceous minerals,(12-14) and formation of interstratified nanocomposite structures for engineering and petrochemical applications.(15-18) Widespread soil radiocesium contamination following the Chernobyl and Fukushima Daiichi nuclear disasters has stimulated research on how micaceous minerals, which bear sites with an extremely high affinity for Cs^+, mediate radiocesium transport. The availability of these high-affinity sites will largely dictate the long-term retention of soil Cs^+, and these sites are thought to be located in the edge and interlayer regions of micas and micaceous clay minerals.(19) Edges have a relatively small exchange capacity, with estimates ranging from ~2%(20) to ~20%(21, 22) of the total cation exchange capacity (CEC) depending on particle size and solution composition. Only a fraction of these (~0.5–10%) are thought to be high-affinity sites.(23) Counterions occupying interlayer regions in micaceous minerals are typically considered inaccessible to exchange, severely limiting the overall availability of high affinity sorption sites for long-term radiocesium immobilization.

Exchange of interlayer K^+ in layered silicates has been studied for more than half a century to understand mica weathering and to quantify overall ion exchange capacities of the layered silicates.(12-14, 24) The key parameters controlling the extent of anhydrous potassium ion exchange (i.e., “weatherability”) include the magnitude of the layer charge, particle size, the identity of the exchanger ion, and the presence of K^+ in solution.(12, 25) Divalent ions and small monovalent ions maintain solvation complexes in the interlayer region, while large monovalent ions such as K^+, Cs^+, and NH_4^+ tend to be anhydrous. Exchange experiments in relatively high structural charge micas and Illite clays have demonstrated that replacement of anhydrous K^+ by hydrated ions of Na^+, Ba^{2+}, and Sr^{2+}(13, 25-28) is kinetically accessible through a hydration mechanism involving significant

clay layer expansion or “decollapse” typical of clay minerals classified as vermiculites. Replacement of interlayer K^+ from micas proceeds inward from the edge, often leaving behind a central core of ions inaccessible to exchange.(29) Nanoscale imaging of the interlayer exchange process in situ has shown that propagation of the exchange front—the interface between nonexchanged and exchanged interlayer regions—is linear in the square root of time, indicating diffusion controlled exchange kinetics.(25) In all prior determinations of interlayer exchange and diffusion kinetics, the exchanger ion has been either been hydrated,(13, 25, 27, 28, 30) or exchange of an anhydrous ion has been mediated by prior exchange by a hydrated ion.(14, 31, 32) In this case, a “collapse-decollapse” kinetic mechanism involving hydrated ion intermediates was assumed to facilitate exchange of Cs^+ in the interlayer region.(30) However, due to strong thermodynamic penalty for replacement of K^+ by hydrated ions in the interlayer,(26) the presence of even trace amounts of aqueous K^+ or NH_4^+ strongly inhibits exchange by solvated counterions,(12, 33) making a decollapse mechanism unlikely under typical environmental conditions. Thus, the underlying microscopic explanation for accessibility of clay interlayers to exchange with anhydrous ions such as Cs^+ and NH_4^+ is effectively unknown.

Direct exchange of anhydrous ions in collapsed interlayers has received very little attention compared with hydrated ion exchange, until recent imaging(34) and spectroscopic(19) studies demonstrated that direct Cs^+ exchange for K^+ in phlogopite and Illite can occur in the absence of a decollapsed intermediate. Exchange of interlayer K^+ for Cs^+ is thermodynamically viable in the presence of aqueous K^+, since the exchange reaction in mica and collapsed clay interlayers is only weakly selective toward K^+.(35, 36, 64) Direct exchange was shown to cause phase separation within individual layers, meaning exchanged layer regions are nearly completely occupied by the exchanging ion (i.e., Cs^+).(34) This picture contrasts sharply with the smoothly varying concentration front expected during diffusion-controlled exchange reactions.(25) The phase separation of ions within a given layer has long been thought to be thermodynamically favored over mixed interlayer structures, but there is no coherent prevailing view to explain how phase separation occurs in general, and multiple pathways are possible.(17, 37) In addition, direct exchange leads to the formation of interstratified structures,(34) where Cs^+-exchanged layers alternate with layers showing little or no penetration of the exchange front. Interstratification is regularly observed in both anhydrous and swelling clays, for both organic(15, 16) and inorganic(14, 17, 31, 38) exchanger ions. Cycles of interlayer expansion and collapse driven by exchange with solvated ions (i.e., Ca^{2+} or Mg^{2+}) followed by K^+ or Cs^+ are thought to induce interstratification, because replacement of K^+ by solvated ions in one layer may strengthen the K^+ binding in the adjacent layers.(14, 26, 31, 32, 39, 40) However, none of the hypothesized pathways can adequately explain

formation of interstratified structures during the direct exchange of K^+ for Cs^+ as observed by Okumura et al.(34)

Here, we use classical molecular dynamics (MD) simulations and density functional theory (DFT) to investigate the mechanism, driving forces and kinetics of direct Cs^+-K^+ exchange in anhydrous interlayers of Illite clay minerals. Classical MD simulations are used to identify the types of migration events responsible for interlayer ion exchange and to quantify the distributions in energy barriers associated with these events, and DFT is used to simulate the energy landscape of interlayer ion diffusion in the vicinity of Cs^+. The combined simulation results provide a detailed understanding of the kinetic phenomena facilitating exchange of Cs^+ for K^+ in Illite and other micaceous minerals.

Simulation Methods

We use both classical atomistic molecular dynamics (MD) and density functional theory (DFT) simulations to understand the mechanisms of interlayer ion exchange in Illite—ubiquitous in shale formations and known to have an extremely high affinity for Cs^+. The MD simulations were performed using the simulation package LAMMPS(41) with customized wrappers to perform high-throughput runs. Interatomic interactions between ions and atoms in Illite were modeled using the ClayFF potential.(42) For layered silicates, ClayFF has been shown to faithfully reproduce ion sorption behavior(43-45) and the dynamics of solvated interlayer ions,(46, 47) but has not been previously tested with respect to ion migration dynamics in anhydrous interlayers. The Climbing Image Nudge Elastic Band (CINEB) method(48) is employed to quantify the diffusion energy barriers in the interlayer, and harmonic transition state theory to evaluate transport rates based on those barriers.(49) For the classical MD simulations, we created an atomic model of multilayer Illite with the structure determined by Gualtieri(50) using X-ray powder diffraction combined with Rietveld and reference intensity ratio methods. This 2:1 phyllosilicate is monoclinic with a chemical formula given by $K_n[Si_{4-n}Al_n]Al_2O_{10}(OH)_2$, where the square brackets indicate Si and Al located in tetrahedrally coordinated sites in the clay layer, with a fraction *n* of tetrahedral Si substituted by Al. This isomorphic substitution creates a negative structural charge compensated by K^+ in the interlayer. Our model Illite ($K_{0.7}[Si_{3.3}Al_{0.7}]Al_2O_{10}(OH)_2$) bears a structural charge of 1.81 mol c/kg, an intermediate value in the non-swelling clays,(51) and contains approximately 30% interlayer site vacancies (Figure 1). The isomorphic substitutions are distributed randomly in the tetrahedral sheet with the restrictions that substitutions cannot occur in neighboring tetrahedral sites.(52) We optimize the K^+ positions for each structure using conjugate gradient potential energy minimization.

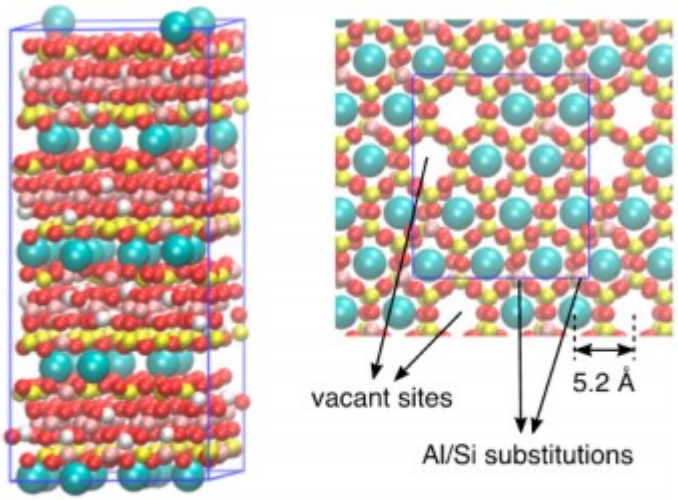

Figure 1. Atomistic illustration of a typical Illite structure used in the molecular dynamics simulations in side (left) and plan (right) view. The K^+ (cyan) located in the interlayer regions compensate the structural charge that arises due to Al^{3+} (pink) substitution for Si^{4+} (yellow) in the tetrahedral sheet of the clay layers. Other elements depicted include oxygen (red) and hydrogen (white).

The DFT simulations are performed at the GGA level of theory with dispersion corrections (revPBE-D3).(53, 54) The systems studied contain 164 atoms (Figure 2a) and are composed of two interlayers, one of which is sampled (Figure 2b). Regardless of the number of isomorphic substitutions, the sampled interlayer contains only one ion (K^+ or Cs^+) to facilitate the sampling. The possible excess of negative charge in the sampled interlayer, e.g. if there is more than one isomorphic substitution, is compensated by the addition of K^+ in the other interlayer such that the net charge of the system is neutral overall. The nonsampled interlayer contains K^+ in all cases. In the main text, we show the results for interlayers where $n = 0.75$, the most representative structure for Illite, although we also studied cases where $n = 0.25$ and 0.5 (Supporting Information, SI). The trends reported for $n = 0.75$ also hold for the other cases. For each value of n, we study 3 distinct scenarios depending on the nature of the ion sampled and the optimized cell dimensions: K^+ in a K^+-optimized cell (i.e., K^+ in K-Illite), Cs^+ in a Cs^+-optimized cell (i.e., Cs^+ in Cs-Illite), and K^+ in a Cs^+-optimized cell (i.e., K^+ in Cs-Illite).

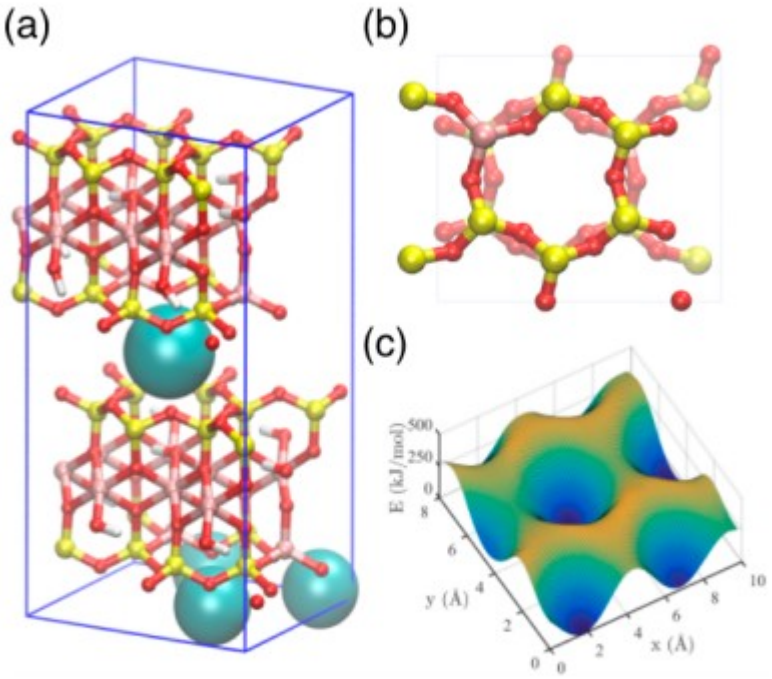

Figure 2. Atomistic illustration of the system used in the DFT simulations. (a) Snapshot of a typical system, where the ions are shown as cyan beads. (2) Plan view of the top and bottom surfaces of the sampled interlayer without the ion. (c) Example of a potential energy surface (PES) reconstructed from DFT energy data.

The protocol that we use to reconstruct the potential energy surface (PES) of K^+ and Cs^+ in the interlayer from DFT calculations is as follows. First, we optimize the simulation cells with either K^+ or Cs^+ in the sampled interlayer using the Broyden-Fletcher-Goldfarb-Shanno (BFGS) algorithm under triclinic symmetry conditions. Once we have the optimal cell parameters, we generate configurations of the system where the *x*–*y* position of the ion in the interlayer is prescribed to a point in a rectangular grid of equispaced points—a total of 378 configurations. For each configuration, the geometry of the system is optimized (with the cell parameters kept constant) and the energy calculated. During the geometry optimization, one Al atom in the octahedral sheet of each layer is constrained, which prevents unphysical translational motions of the layers. The ion is constrained at the prescribed positions in the *x*–*y* directions, but it is allowed to relax in the direction perpendicular to the surface. The PES is then reconstructed from the DFT energy data points using a biharmonic interpolation scheme (Figure 2c). Finally, we calculate the minimum energy paths (MEP) connecting the different local minima in the landscape using the zero-temperature string method (ZTS),(55, 56) which is adequate given the smoothness of the PES. Additional technical details regarding the computational methods are provided in the SI.

Results and Discussion

Classical Molecular Simulations of Interlayer Energetics and Ion Dynamics

Clay minerals contain vacancies at interlayer sites in inverse proportion to the magnitude of the structural charge. These vacancies facilitate mass transport through the interlayer and are therefore critical to the process of interlayer ion exchange. In order to have a representative system, it is important to optimize the positions of ions and vacancies in the interlayer. Figure 3a shows the distribution of cohesive energies of interlayer cations before (gray) and after (black) optimization of their positions in the interlayer. We find that interlayer K^+ counterions prefer local charge deficit regions adjacent to greater numbers of Si–Al isomorphic substitutions (Figure 3b). Thus, layers with locally higher densities of substitutions are likely to contain more counterions and fewer vacancies, indicating that counterion distributions are likely nonrandom.(10)

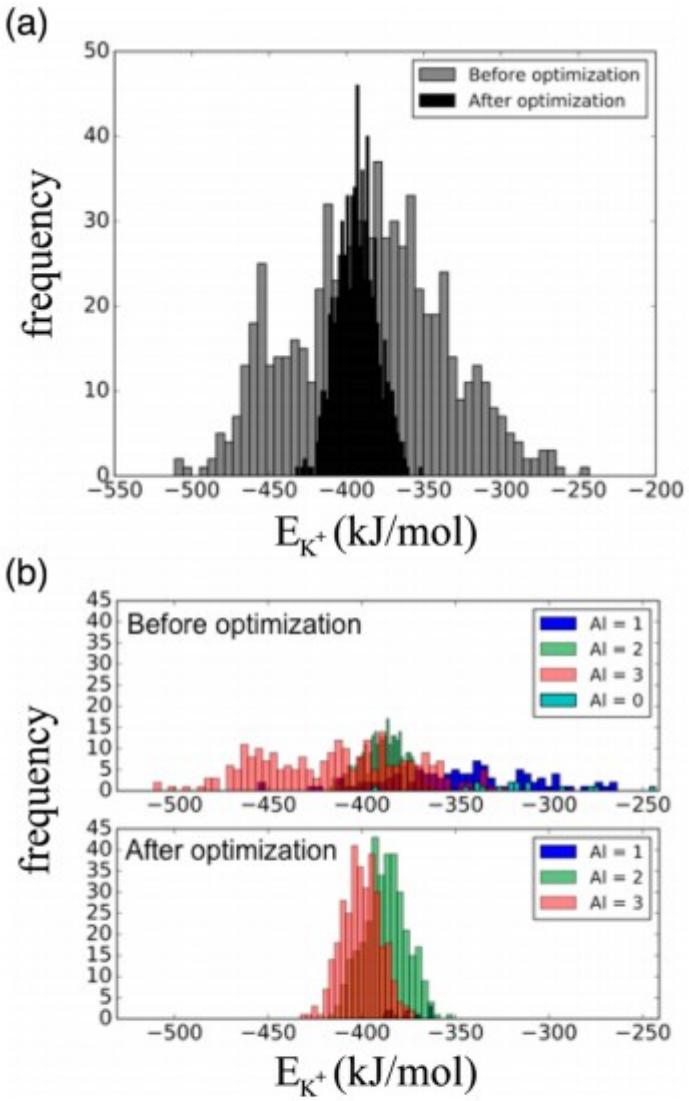

Figure 3. (a) Distribution of cohesive energies of interlayer K^+ before (gray) and after (black) optimization for their positions in the interlayer, (b) distribution of K^+ cohesive energies segmented by the number of Al^{3+} nearest neighbors before and after optimization The analyses of variance between and within the groups gives F-statistic as 234.65 ($p = 0$) for $n = 664$, suggesting that the probability that these distributions arise from random, otherwise similar groups, is almost impossible.

Initially, brute force molecular dynamics (MD) simulations using the ClayFF force field were performed for temperatures between 500 and 900 K to determine whether interlayer ion migration is observable over nanosecond time scales in K-Illite. No migration of the interlayer K^+ was observed (SI Figure S1), which suggests that the barrier for migration is too high to directly observe over MD time scales, even at elevated temperatures. Instead, we use the CINEB method to investigate the kinetics of single interlayer ion migration events or hops from occupied to adjacent vacant

counterion sites. These elementary steps collectively control the diffusion of interlayer ions and the propagation of ion exchange fronts. CINEB is used to determine the lowest energy path and calculate the energy barriers associated with interlayer ion migration events. Since the local environment around each K^+ is variable—for example, different numbers of neighboring tetrahedral Al and K^+—we expect there to be a distribution of K^+ migration barriers. In order to capture this distribution, we calculated barriers for an ensemble of several hundred K^+ migrating to all their possible vacant neighboring sites.

The green line in Figure 4a shows a typical path followed by a migrating K^+ after optimization of the initial assumed path (black line), in which the K^+ moves past the oxygen ion at the center of the line joining two stable sites. Figure 4b shows a representative migration barrier, where the *x*-axis reaction coordinate is scaled such that 0 corresponds to one stable site and 1 corresponds to another adjacent, initially vacant, counterion site. In this particular example, the barrier for the forward migration is ~250 kJ/mol with the final state ~10 kJ/mol higher in energy than the initial state. Figure 4c shows a distribution of migration barriers for over 650 cases studied, including reverse migration barriers. For the ground state K-Illite structure, we calculate a mean barrier to interlayer ion migration of 226 ± 51 kJ/mol (1σ). Migration events with such large energy barriers cannot be directly observed in conventional MD simulations unless the migration attempt frequencies are orders of magnitude greater than the Einstein frequency (10^{11}–10^{14} s^{-1}), which is typical for single-atom led migrations/transitions in solids. While it is possible for migrations/transitions to have large effective attempt frequencies, such large frequencies are usually only observed for collective processes involving the simultaneous motion of many atoms.(57)

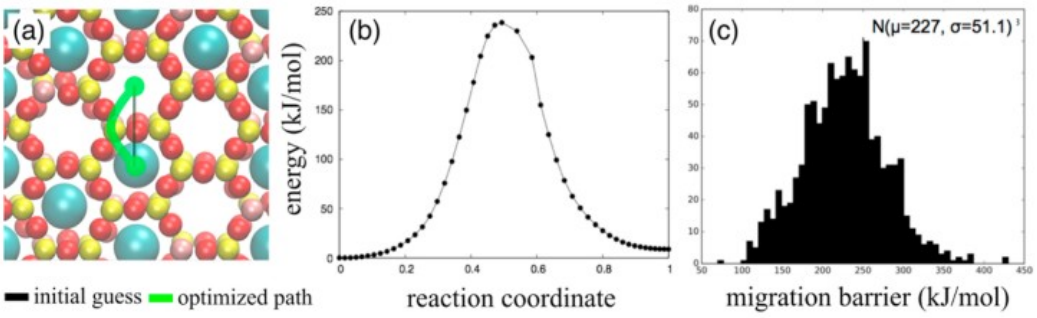

Figure 4. Results of a typical CINEB calculation with the optimized ion migration path (a) and its corresponding energy barrier (b). A histogram summarizing several hundred CINEB results (c) gives a mean energy barrier of 227 ± 102 kJ/mol (95% of data) for K^+ ion migration from occupied sites to neighboring vacant sites.

The considerable observed variability in the magnitude of the migration barrier requires further discussion. If we assume that the migration path and mechanism itself remains the same for all migration events, we can attribute this variation in part to differences in the cohesive energies of K^+ at stable sites. A simple regression analysis of the data suggests that we can expect about 0.5 kJ/mol increase in barrier for 1 kJ/mol increase in cohesive energy

of the stable site (SI Figure S2). These findings demonstrate for the first time a mechanism by which local charge distribution can influence interlayer reaction kinetics. Other potential sources of variability, such as the migration direction (SI Figure S3), have a statistically insignificant impact on the migration barrier. In general, we expect ClayFF to underestimate the true magnitude of the migration barrier, due to the nonbonded nature of the force field that makes structures excessively deformable.(58, 59)

Interlayer K^+ Diffusion Dynamics: Comparison with Experiment

Despite the wide range in calculated migration barriers, the values are far too high to explain the amount of exchange observed experimentally, where the exchange front between Cs^+ and K^+ is observed to propagate by at least tens of nanometers over 1 year time scales in Illite(19) and by a similar distance over 24 h time scales in K-phlogopite.(34) This can be shown by simple arguments. Assuming ions diffuse in the interlayer following a random walk, the mean squared displacement (MSD) scales as $\langle r^2 \rangle = a^2 N$ (1) where N is the number of hops and a is the lattice spacing. The value of N depends on elapsed time (t, s) following: [redacted] (2) where ν_0 is the frequency of ion vibration in the minima, E_a is the magnitude of the energy barrier for a single hop, R is the gas constant (0.008314 kJ/mol K), and T is absolute temperature (K). For reasonable values of these parameters ($\nu_0 = 10^{13}$ s^{-1}, a = 5.2 Å, t = 1 year, and T = 298 K), the CINEB calculated migration barriers correspond to a root MSD of 1.4×10^{-19} m, and a range based on the 1σ uncertainty in the migration barrier of 4.2×10^{-15} m to 4.9×10^{-21} m. These displacement distances are significantly smaller than even the distances separating stable counterion sites in the Illite structure (5.2×10^{-10} m). Thus, based on these migration barriers, we estimate that the self-diffusion of K^+ in ground state ClayFF Illite is far too slow to permit the extent of exchange observed in experiments. In addition, our calculated migration barriers are significantly higher than values estimated for the diffusion of solvated Na^+ into K-phlogopite,(25) which may be limited by the mobility of K^+ at the exchange front. In fact, the largest reported barrier to hydrated ion exchange with K^+ in mica is ~106 kJ/mol,(26) significantly less than the average of our barrier distribution shown in Figure 4c.

Electronic Structure Calculations of Interlayer Energetics

Given the apparent mismatch with experiments, electronic structure DFT calculations were performed to verify that the calculated barriers and mechanistic assumptions based on the ClayFF force field are reasonable. The results are shown for n = 0.75 in Figure 5, with additional results in SI Figures S4 and S5, for n = 0.25 and n = 0.5 respectively. Overall, the magnitude of the energy barriers associated with K^+ migration in K-Illite (Figure 5a) averaged over all orientations is 317 ± 36 kJ/mol (1σ), which is approximately 30% higher than the energy barrier calculated from the CINEB simulations using ClayFF. The DFT simulations show two distinct pathways of

ion migration between occupied and vacant interlayer sites. The first is in agreement with the CINEB calculations and connects two minima following a curved path that avoids the oxygen between tetrahedrally coordinated Si or Al (Figure 5a–c). The second pathway is a straight line between the two minima and occurs only in the horizontal direction (*a*-axis crystal orientation). These linear pathways, which ClayFF fails to identify, exhibit substantially lower energy barriers (by around 40–70 kJ/mol) than the curved paths (Figure 5a–c), suggesting that ion exchange rates in single crystals may be anisotropic. Existing experimental evidence for the exchange front structure is inconclusive: in a recent study, in situ imaging of Na^+–K^+ exchange in phlogopite appears to show slightly elongated (oval) exchange front structures originating at defects on the scale of a single layer,(25) whereas in an older study, optical imaging gives no evidence of exchange front anisotropy in biotite on the scale of a single crystal.(29) Inspection of the clay structure reveals that the Al atoms in the octahedral sheet may be mechanically reinforcing the straight diagonal pathways, forcing the ion to take the alternative curved path (SI Figure S6). The inability of ClayFF to capture this behavior may lay in the fact that it fails to reproduce the ditrigonal geometry of the cavities in the surface of the tetrahedral sheet (SI Figure S7), and also on its inadequate representation of the mechanical properties of layered silicates.(58, 59) Layer stacking may also influence the occurrence of exchange front anisotropy, which may explain why it can be observed in a single layer but not in a single crystal.

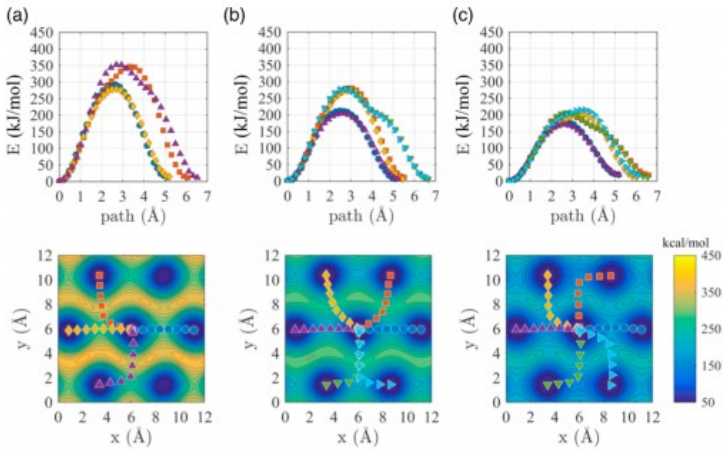

Figure 5. Minimum energy paths (MEP) found on the DFT-reconstructed potential energy surfaces (PES). Top-plots show the energy along the different paths, and bottom-plots show the actual path over the PES. (a) K^+ in K-Illite, (b) Cs^+ in Cs-Illite, and (c) K^+ in Cs-Illite.

Somewhat surprisingly, these calculations show no discernible dependence of the energy barriers on structural charge (Figure 5 versus SI Figures S4 and S5), which is likely due to the fact that these barriers are controlled by the physical width of the interlayer and thus the size of the counterion. Experiments suggest that exchange of interlayer ions proceeds more rapidly in phases with lower structural charge when driven by a decollapse mechanism,(12, 30) but these results are not directly comparable to the

direct exchange process investigated here. There are no studies to the authors' knowledge investigating the impact of layer charge on rates of ion exchange in anhydrous interlayers. We hypothesize that in the case of interlayers with a large number of interlayer vacancies (i.e., low structural charge), the direct exchange process is likely to be limited by individual migration events, and hence the diffusion energy barriers. However, in the case of interlayers with very high structural charge, where the number of vacancies is minimal, the exchange process will likely be limited instead by the diffusion of vacancies themselves. In this case, exchange rates are expected to be largely independent of the diffusion energy barriers to single ion migration events. This emergent behavior as a function of the interlayer occupancy, or structural charge, merits further research.

Chemical-Mechanical Coupling as a Driver for Exchange

The results of these DFT calculations reinforce our conclusion that the ion migration barriers of K^+ in ground state K-Illite are far too high to explain observed Cs^+-K^+ exchange dynamics. Thus, an alternative mechanism must be invoked to explain the observed exchange phenomena. Upon close inspection, we find that the exchange reaction alters the structure of the interlayer to accommodate the larger size of Cs^+ with respect to K^+, making the interlayer in the vicinity of a Cs^+ larger than for K^+. The ClayFF model predicts a linear increase in the interlayer spacing with Cs^+ substitution for K^+ (SI Figure S8), and the interlayer spacing of the Cs-Illite end member is 0.67 ± 0.03 Å larger than that of pure K-Illite. Similarly, the DFT calculations predict in increase of the interlayer spacing of 0.75 Å between K- and Cs-Illite end-members, consistent with measured values.(19, 34) Since the maximum of the energy barrier predicted by both atomistic and ab initio methods is controlled by the position of oxygen atoms that delineate the ditrigonal cavities, increasing the width of the interlayer region is likely to decrease the magnitude of the barrier. We hypothesize the existence of a molecular mechanism involving larger exchanging ions, such as Cs^+, that lowers the migration barrier for K^+. The increment in interlayer spacing provided by neighboring Cs^+ ions likely reduces the migration barrier for K^+ at the exchange front, leading to a positive-feedback exchange mechanism that accelerates subsequent exchange and migration events.

Both DFT and ClayFF CINEB results support this positive feedback hypothesis. Using DFT, we observe that the average energy barrier of K^+ in Cs-Illite (Figure 5c)—a realistic scenario for a K^+ ion located at the front of the exchange process, where it has a substantial percentage of Cs^+ neighbors—drops dramatically by 125 kJ/mol (from 317 to 192 kJ/mol). Similarly, the mode of the distribution of activation energy barriers for ion migration calculated using CINEB with ClayFF decreases linearly with increasing Δd (Figure 6). Complete substitution of K^+ by Cs^+ is expected to lower the barrier for K^+ migration at the exchange front to approximately 150 kJ/mol (SI Figure S9). The local increase in interlayer spacing caused by Cs^+ exchange for K^+ lowers the energy barrier for K^+ ion migration, leading to

an exponential increase in K^+ diffusivity. According to eqs 1 and 2, the decrease in barriers predicted by atomistic and ab initio simulation results would yield an expected increase in the K^+ ion migration kinetics by 6 and 10 orders of magnitude, respectively. These results provide evidence of a new mechanism for direct exchange of anhydrous ions that arises from the interplay between interlayer structure and reactivity (i.e., "chemical-mechanical coupling") and that does not require intermediate swelling states (decollapse) to occur.

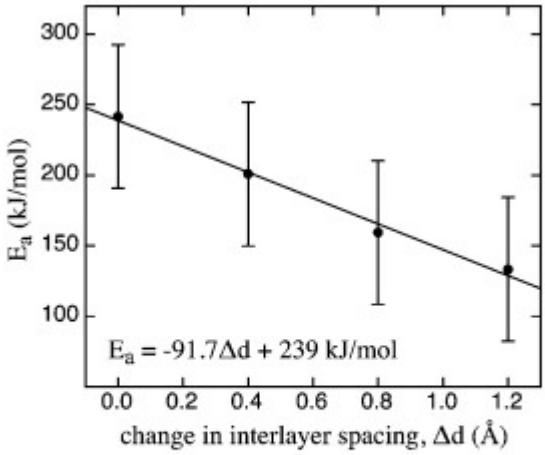

Figure 6. Magnitude of the K^+ migration barrier decreases linearly with increasing interlayer spacing, from the K-Illite end-member (Δd = 0 Å) to layer spacings typical of the Cs-Illite end-member (Δd = 0.67 ± 0.03 Å).

Formation of Phase-Separated Interlayers

Experimental observations of the structure of the exchange front show that it is sharp, instead of a smooth, diffusive interface, and that the Cs^+ substituted region is almost completely clear of K^+.(34) The positive-feedback exchange mechanism proposed here explains why a sharp front will facilitate K^+ exchange (i.e., K^+ is only highly mobile in the vicinity of Cs^+) but does not fully elucidate the near-complete exchange that is observed. To explain this behavior, we evaluated the thermodynamic driving force for Cs- and K-Illite phase separation by calculating the change in free energy as a function of the mole fraction of Cs^+ randomly mixed in the interlayer. Based on an ensemble of ClayFF energy minimization calculations, we find that there is a significant energetic penalty for mixing small amounts of Cs^+ in K-Illite interlayers and vice versa (SI Figure 10). For example, replacing 10% of the K^+ by Cs^+ results in a per-molar free energy penalty of 13.2 ± 6.0 kJ/mol. Thus, the demixing of Cs^+ and K^+ in the interlayer is strongly favored. We conclude that both the bulk phase thermodynamics and the kinetic feedbacks associated with Cs^+-K^+ exchange lead to the formation of phase-separated interlayer regions. Thermodynamically favorable phase-separated domains naturally arise even in the absence of a heterogeneous layer charge

distribution, which has long been invoked to explain the prevalence of these structures in clays.(60)

Additional Factors Influencing Interlayer Exchange Kinetics

Despite some quantitative discrepancies between DFT and ClayFF, both methods capture the trend that supports our hypothesized molecular mechanism for promoting the K^+/Cs^+ exchange. It is worth noting that the energy barriers reported here refer to potential energy, and although we do not expect entropy to play a major role in the process due to the large binding energies involved, it is important to keep in mind that these are upper limits to the real free energy barriers. While it is possible that the presence of trace interlayer water or structural defects could accelerate K^+ migration, it is not necessary to invoke these phenomena to explain the observed direct exchange dynamics. The feedback between interlayer structure and exchange kinetics—chemical–mechanical coupling—is sufficient to explain the direct exchange of Cs^+ for K^+ in micaceous minerals.

Additional geochemical factors such as the composition of the aqueous solution and the structure and protonation state of the edge will play a role in mediating the macroscopic kinetics of the exchange reaction, but these are unlikely to alter the basic molecular mechanism driving the exchange. Formation of interstratified structures in which substituted layers randomly alternate with pristine layers may arise as a consequence of mechanical interactions between layers, which promote exchange in some layers at the expense of others, and the dynamics of this process will be the focus of a future study.

Environmental Significance

The accessibility of interlayer sites to exchange implies that the ion exchange capacity of non-swelling clays, those that have an extremely high affinity for radiocesium, may be significantly greater than expected based on standard short-term (often 24 h) exchange experiments. It is likely that ions of similar size and charge to K^+, also including NH_4^+, can undergo direct exchange with micaceous clay interlayers in the absence of an expanded intermediate. Indeed, redox gradients in the environment can generate high concentrations of NH_4^+ in pore fluids, which in turn can remobilize Illite-bound radiocesium.(61) The contribution of the clay interlayer specifically to such ion exchange driven remobilization has not been established.

In addition to their role in regulating radiocesium transport, non-swelling clay minerals control the availability of critical soil nutrients, K^+ and NH_4^+.(24, 27, 62) Given the slight thermodynamic preference of the interlayer for K^+ relative to species of like size and charge, direct exchange reactions can proceed even in the presence of aqueous K^+, which is known to inhibit interlayer ion exchange in the swelling clays.(28, 63) Thus, we expect the long-term transport behavior of these species in the environment to be controlled at least in part by exchange reactions involving micaceous clay

interlayers. Because these phases dominate the clay mineral fraction of sedimentary rocks globally, collapsed interlayers may in fact constitute a reservoir of ion exchange capacity that has been largely overlooked. Direct anhydrous interlayer ion exchange could play a significant role in regulating the mass transport of nutrients and radionuclides in the environment and thus merits further study.

Acknowledgments

The Laboratory Directed Research and Development Program of Lawrence Berkeley National Laboratory supported this work under U.S. Department of Energy Contract No. DE-AC02-05CH11231. This research used resources of the National Energy Research Scientific Computing Center, a DOE Office of Science User Facility supported by the Office of Science of the U.S. Department of Energy under Contract No. DE-AC02-05CH11231.

References

(1) Evans, D. W.; Alberts, J. J.; Clark, R. A. Reversible ion-exchange fixation of cesium-137 leading to mobilization from reservoir sediments. Geochim. Cosmochim. Acta 1983, 47 (6), 1041−1049.

(2) Anderson, S. J.; Sposito, G. Cesium-Adsorption Method for Measuring Accessible Structural Surface Charge. Soil Science Society of America Journal 1991, 55 (6), 1569−1576.

(3) Hinton, T. G.; Kaplan, D. I.; Knox, A. S.; Coughlin, D. P.; Nascimento, R. V.; Watson, S. I.; Fletcher, D. E.; Koo, B.-J. Use of Illite clay for in situ remediation of 137Cs-contaminated water bodies: field demonstration of reduced biological uptake. Environ. Sci. Technol. 2006, 40 (14), 4500−4505.

(4) Bourg, I.; Sposito, G. Ion exchange phenomena. In Handbook of Soil Science, Properties, and Processes, 2nd ed.; Huang, P., Li, Y., Sumner, M., Eds.; CRC Press, 2011.

(5) Tachi, Y.; Yotsuji, K.; Seida, Y.; Yui, M. Diffusion and sorption of Cs+, I− and HTO in samples of the argillaceous Wakkanai Formation from the Horonobe URL, Japan: Clay-based modeling approach. Geochim. Cosmochim. Acta 2011, 75 (22), 6742−6759.

(6) Gaboreau, S.; Claret, F.; Crouzet, C.; Giffaut, E.; Tournassat, C. Caesium uptake by Callovian−Oxfordian clayrock under alkaline perturbation. Appl. Geochem. 2012, 27 (6), 1194−1201.

(7) Chen, Z.; Montavon, G.; Ribet, S.; Guo, Z.; Robinet, J.; David, K.; Tournassat, C.; Grambow, B.; Landesman, C. Key factors to understand in-situ behavior of Cs in Callovo−Oxfordian clay-rock (France). Chem. Geol. 2014, 387, 47−58.

(8) Fan, Q.; Tanaka, M.; Tanaka, K.; Sakaguchi, A.; Takahashi, Y. An EXAFS study on the effects of natural organic matter and the expandability of clay

minerals on cesium adsorption and mobility. Geochim. Cosmochim. Acta 2014, 135, 49−65.

(9) Mukai, H.; Hatta, T.; Kitazawa, H.; Yamada, H.; Yaita, T.; Kogure, T. Speciation of radioactive soil particles in the Fukushima contaminated area by IP autoradiography and microanalyses. Environ. Sci. Technol. 2014, 48 (22), 13053−13059.

(10) Ngouana, W. B. F.; Kalinichev, A. G. Structural arrangements of isomorphic substitutions in smectites: Molecular simulation of the swelling properties, interlayer structure, and dynamics of hydrated Cs−montmorillonite revisited with new clay models. J. Phys. Chem. C 2014, 118 (24), 12758−12773.

(11) Loganathan, N.; Yazaydin, A. O.; Bowers, G. M.; Kalinichev, A. G.; Kirkpatrick, R. J. Structure, Energetics, and Dynamics of Cs+ and H2O in Hectorite: Molecular Dynamics Simulations with an Unconstrained Substrate Surface. J. Phys. Chem. C 2016, 120 (19), 10298−10310.

(12) Scott, A.; Smith, S. Susceptibility of Interlayer Potassium in Micas to Exchange with Sodium. In Clays and Clay Minerals: Proceedings of the Fourteenth National Conference, Berkeley, California; Elsevier, 1966; pp 69−80.

(13) Reichenbach, H.; Rich, C. Potassium release from muscovite as influenced by particle size. Clays Clay Miner. 1969, 17, 23−29.

(14) Sawhney, B. Selective sorption and fixation of cations by clay minerals: a review. Clays Clay Miner. 1972, 20 (9), 93−100.

(15) Barrer, R.; Brummer, K. Relations between partial ion exchange and interlamellar sorption in alkylammonium montmorillonites. Trans. Faraday Soc. 1963, 59, 959−968.

(16) Theng, B.; Greenland, D.; Quirk, J. Adsorption of alkylammonium cations by montmorillonite. Clay Miner. 1967, 7 (1), 1−17.

(17) Nadeau, P.; Wilson, M.; McHardy, W.; Tait, J. Interstratified clays as fundamental particles. Science 1984, 225, 923−925.

(18) Suter, J. L.; Groen, D.; Coveney, P. V. Mechanism of Exfoliation and Prediction of Materials Properties of Clay−Polymer Nanocomposites from Multiscale Modeling. Nano Lett. 2015, 15 (12), 8108−8113.

(19) Fuller, A. J.; Shaw, S.; Ward, M. B.; Haigh, S. J.; Mosselmans, J. F. W.; Peacock, C. L.; Stackhouse, S.; Dent, A. J.; Trivedi, D.; Burke, I. T. Caesium incorporation and retention in Illite interlayers. Appl. Clay Sci. 2015, 108, 128−134.

(20) Poinssot, C.; Baeyens, B.; Bradbury, M. H. Experimental and modelling studies of caesium sorption on Illite. Geochim. Cosmochim. Acta 1999, 63 (19−20), 3217−3227.

(21) Benedicto, A.; Missana, T.; Fernandez, A. M. Interlayer collapse´ affects on cesium adsorption onto Illite. Environ. Sci. Technol. 2014, 48 (9), 4909−4915.

(22) Tamura, K.; Kogure, T.; Watanabe, Y.; Nagai, C.; Yamada, H. Uptake of Cesium and Strontium Ions by Artificially Altered Phlogopite. Environ. Sci. Technol. 2014, 48 (10), 5808−5815.

(23) Wauters, J.; Sweeck, L.; Valcke, E.; Elsen, A.; Cremers, A. Availability of radiocaesium in soils: a new methodology. Sci. Total Environ. 1994, 157, 239−248.

(24) Barshad, I. Cation exchange in micaceous minerals: II. Replaceability of ammonium and potassium from vermiculite, biotite, and montmorillonite. Soil Sci. 1954, 78 (1), 57−76.

(25) Sanchez-Pastor, N.; Aldushin, K.; Jordan, G.; Schmahl, W. W. K´ +−Na+ exchange in phlogopite on the scale of a single layer. Geochim. Cosmochim. Acta 2010, 74 (7), 1954−1962.

(26) Rausell-Colom, J.; Sweatman, T.; Wells, C.; Norrish, K. Studies in the artificial weathering of mica. Exper. Pedol. 1965, 40−72.

(27) Quirk, J.; Chute, J. Potassium Release from Mica-Like Clay Minerals. In 9th International Congress of Soil Science Transactions; Holmes, J. W., Ed. International Society of Soil Science: Adelaide, Australia, 1968; Vol. 2, pp 671−681.

(28) Reichenbach, H.; Rich, C. Preparation of dioctahedral vermiculites from muscovite and subsequent exchange properties. In 9th International Congress of Soil Science Transactions, Holmes, J. W., Ed.; International Society of Soil Science, 1968; Vol. 1, pp 709−719.

(29) Scott, A. Effect of particle size on interlayer potassium exchange in micas. In 9th International Congress of Soil Science Transactions,; Holmes, J. W., Ed.; International Society of Soil Science: Adelaide, Australia, 1968; Vol. 2, pp 649−658.

(30) Lai, T.; Mortland, M. Diffusion of ions in bentonite and vermiculite. Soil Science Society of America Journal 1961, 25 (5), 353− 357.

(31) Sawhney, B. Interstratification in vermiculite. Clays Clay Miner. 1967, 15, 75−84.

(32) Sawhney, B. Regularity of interstratification as affected by charge density in layer silicates. Soil Science Society of America Journal 1969, 33 (1), 42−46.

(33) Scott, A.; Hunziker, R.; Hanway, J. Chemical extraction of potassium from soils and micaceous minerals with solutions containing sodium tetraphenylboron. I. Preliminary experiments. Soil Science Society of America Journal 1960, 24 (3), 191−194.

(34) Okumura, T.; Tamura, K.; Fujii, E.; Yamada, H.; Kogure, T. Direct observation of cesium at the interlayer region in phlogopite mica. Microscopy 2014, 63 (1), 65−72.

(35) Okumura, M.; Nakamura, H.; Machida, M. Mechanism of strong affinity of clay minerals to radioactive cesium: first-principles calculation study for adsorption of cesium at frayed edge sites in muscovite. J. Phys. Soc. Jpn. 2013, 82 (3), 033802.

(36) Suehara, S.; Yamada, H. Cesium stability in a typical mica structure in dry and wet environments from first-principles. Geochim. Cosmochim. Acta 2013, 109, 62−73.

(37) Xu, S.; Boyd, S. A. Cation exchange chemistry of hexadecyltrimethylammonium in a subsoil containing vermiculite. Soil Science Society of America Journal 1994, 58 (5), 1382−1391.

(38) Kogure, T.; Morimoto, K.; Tamura, K.; Sato, H.; Yamagishi, A. XRD and HRTEM evidence for fixation of cesium ions in vermiculite clay. Chem. Lett. 2012, 41 (4), 380−382.

(39) Bassett, W. A. The origin of the vermiculite deposit at Libby, Montana. Am. Mineral. 1959, 44 (3−4), 282−299.

(40) Farmer, V.; Wilson, M. Experimental conversion of biotite to hydrobiotite. Nature 1970, 226, 841.

(41) Plimpton, S. Fast parallel algorithms for short-range molecular dynamics. J. Comput. Phys. 1995, 117 (1), 1−19.

(42) Cygan, R. T.; Liang, J.-J.; Kalinichev, A. G. Molecular models of hydroxide, oxyhydroxide, and clay phases and the development of a general force field. J. Phys. Chem. B 2004, 108 (4), 1255−1266.

(43) Bourg, I. C.; Sposito, G. Connecting the molecular scale to the continuum scale for diffusion processes in smectite-rich porous media. Environ. Sci. Technol. 2010, 44 (6), 2085−2091.

(44) Ferrage, E.; Sakharov, B. A.; Michot, L. J.; Delville, A.; Bauer, A.; Lanson, B.; Grangeon, S.; Frapper, G.; Jimenez-Ruiz, M.; Cuello, G. J.´ Hydration Properties and Interlayer Organization of Water and Ions in Synthetic Na-Smectite with Tetrahedral Layer Charge. Part 2. Toward a Precise Coupling between Molecular Simulations and Diffraction Data. J. Phys. Chem. C 2011, 115 (5), 1867−1881.

(45) Marry, V.; Dubois, E.; Malikova, N.; Durand-Vidal, S.; Longeville, S.; Breu, J. Water dynamics in hectorite clays: Infuence of temperature studied by coupling neutron spin echo and molecular dynamics. Environ. Sci. Technol. 2011, 45 (7), 2850−2855.

(46) Holmboe, M.; Bourg, I. C. Molecular dynamics simulations of water and sodium diffusion in smectite interlayer nanopores as a function of pore size and temperature. J. Phys. Chem. C 2013, 118 (2), 1001−1013.

(47) Tertre, E.; Delville, A.; Pret, D.; Hubert, F.; Ferrage, E. Cationˆ diffusion in the interlayer space of swelling clay minerals−A combined macroscopic and microscopic study. Geochim. Cosmochim. Acta 2015, 149, 251−267.

(48) Henkelman, G.; Uberuaga, B. P.; Jonsson, H. A climbing image´ nudged elastic band method for finding saddle points and minimum energy paths. J. Chem. Phys. 2000, 113 (22), 9901−9904.

(49) Vineyard, G. H. Frequency factors and isotope effects in solid state rate processes. J. Phys. Chem. Solids 1957, 3 (1−2), 121−127.

(50) Gualtieri, A. F. Accuracy of XRPD QPA using the combined Rietveld−RIR method. J. Appl. Crystallogr. 2000, 33 (2), 267−278.

(51) Sposito, G. The Chemistry of Soils. Oxford University Press, 2008.

(52) Sainz-Diaz, C.; Cuadros, J.; Hernandez-Laguna, A. Analysis of´ cation distribution in the octahedral sheet of dioctahedral 2:1 phyllosilicates by using inverse Monte Carlo methods. Phys. Chem. Miner. 2001, 28 (7), 445−454.

(53) Grimme, S.; Antony, J.; Ehrlich, S.; Krieg, H. A consistent and accurate ab initio parametrization of density functional dispersion correction (DFT-D) for the 94 elements H-Pu. J. Chem. Phys. 2010, 132 (15), 154104.

(54) Zhang, Y.; Yang, W. Comment on “Generalized gradient approximation made simple. Phys. Rev. Lett. 1998, 80 (4), 890.

(55) Weinan, E.; Ren, W.; Vanden-Eijnden, E. Simplified and improved string method for computing the minimum energy paths in barrier-crossing events. J. Chem. Phys. 2007, 126 (16), 164103.

(56) Weinan, E.; Ren, W.; Vanden-Eijnden, E. String method for the study of rare events. Phys. Rev. B: Condens. Matter Mater. Phys. 2002, 66 (5), 052301.

(57) Uberuaga, B.; Hoagland, R.; Voter, A.; Valone, S. Direct transformation of vacancy voids to stacking fault tetrahedra. Phys. Rev. Lett. 2007, 99 (13), 135501.

(58) Shahsavari, R.; Pellenq, R. J.-M.; Ulm, F.-J. Empirical force fields for complex hydrated calcio-silicate layered materials. Phys. Chem. Chem. Phys. 2011, 13 (3), 1002−1011.

(59) Teich-McGoldrick, S. L.; Greathouse, J. A.; Cygan, R. T. Molecular dynamics simulations of structural and mechanical properties of muscovite: pressure and temperature effects. J. Phys. Chem. C 2012, 116 (28), 15099−15107.

(60) Vali, H.; Koster, H. Expanding behaviour, structural disorder, regular and random irregular interstratification of 2:1 layer-silicates studied by high-resolution images of transmission electron microscopy. Clay Miner. 1986, 21 (5), 827−859.

(61) Comans, R. N. J.; Middelburg, J. J.; Zonderhuis, J.; Woittiez, J. R. W.; Lange, G. J. D.; Das, H. A.; Weijden, C. H. V. D. Mobilization of radiocaesium in pore water of lake sediments. Nature 1989, 339 (6223), 367−369.

(62) Smith, S. J.; Clark, L. J.; Scott, A. D. Exchangeability of potassium in soils. In 9th International Congress of Soil Science Transactions; Holmes, J. W., Ed.; International Society of Soil Science: Adelaide, Australia, 1968; Vol. 2, pp 661−670.

(63) Boek, E. S.; Coveney, P. V.; Skipper, N. T. Monte Carlo molecular modeling studies of hydrated Li-, Na-, and K-smectites: Understanding the role of potassium as a clay swelling inhibitor. J. Am. Chem. Soc. 1995, 117 (50), 12608−12617.

(64) Lammers, L. N.; Bourg, I. C.; Okumura, M.; Kolluri, K.; Sposito, G.; Machida, M. Molecular dynamics simulations of cesium adsorption on illite nanoparticles. J. Colloid Interface Sci. 2017, 490 (490), 608− 620.